Cambridge Centre for Computational Chemical Engineering

University of Cambridge

Department of Chemical Engineering

Preprint ISSN 1473 – 4273

Numerical simulation and sensitivity analysis of detailed soot particle size distribution in laminar premixed ethylene flames

Jasdeep Singh, Robert I A Patterson, Markus Kraft[1], Hai Wang[2]

submitted: August 9, 2005

[1] Department of Chemical Engineering
University of Cambridge
Pembroke Street
Cambridge CB2 3RA
UK
E-mail: markus_kraft@cheng.cam.ac.uk

[2] Department of Aerospace and Mechanical Engineering
University of Southern California
Los Angeles, California 90089-1453
USA
E-mail: haiw@usc.edu

Preprint No. 29

c4e

Key words and phrases. Soot, Particle size distribution, Premixed flames.

Edited by
Cambridge Centre for Computational Chemical Engineering
Department of Chemical Engineering
University of Cambridge
Cambridge CB2 3RA
United Kingdom.

Fax: + 44 (0)1223 334796
E-Mail: c4e@cheng.cam.ac.uk
World Wide Web: http://www.cheng.cam.ac.uk/c4e/

Abstract

In this paper, the prediction of a soot model [Appel *et. al*, Combustion and Flame, 121(2000)] is compared to recently a published set of highly detailed soot particle size distributions [Zhao *et. al*, Proceedings of Combustion Institute, 30(2005)]. A stochastic approach is used to obtain soot particle size distributions (PSDs). The key features of the measured and simulated particle size distributions are identified and used as a simple way of comparing PSDs. The sensitivity of the soot PSDs to the parameters defining parts of the soot model, such as soot inception, particle and PAH collision efficiency and enhancement, and surface activity is investigated. Incepting soot particle size is found to have a very significant effect on the lower end of the PSDs, especially the position of the trough for a bimodal soot PSDs. A new model for the decay in the surface activity is proposed in which the activity of the soot particle depends only on the history of that particle and the local temperature in the flame. This is a first attempt to use local flame variables to define the surface ageing which has major impact on the prediction of high end of the PSDs. Using these modifications to the soot model it is possible to improve the agreement between some of the points of interest in the simulated and measured PSDs. The paper achieves the task to help advance the soot models to predict soot PSD in addition to soot volume fraction and number density, which has been the focus of the literature.

Contents

1 Introduction **3**

2 Experimental Data Analysis **4**

3 Numerical Details **6**

4 Numerical Results **7**

5 Numerical Sensitivity Analysis **11**

5.1 Sticking Probability of Pyrene-Pyrene Collision 11

5.2 Sticking Probability of PAH-Particle Collision 13

5.3 Density of Active Surface Sites 13

5.4 Assumption of "Smallest" Model Particle 16

5.5 Particle-Particle Coagulation: Effect of Van der Waals Enhancement Factors 18

6 Conclusion **20**

1 Introduction

Understanding the mechanisms of soot formation is a long standing challenge in combustion research. Quantitative knowledge of soot formation has been largely derived from three types of work: measurement of soot volume fraction, number density and particle size distributions (PSD) [1, 2, 3, 4, 5, 6, 7, 8]; development of detailed chemical mechanisms for the formation of polycyclic aromatic hydrocarbons [9, 10, 11, 12, 13, 14, 15, 16]; and development of soot population dynamics models to describe the evolution of the particle ensemble [5, 9, 10, 13, 17, 18, 19, 20, 21, 22, 23, 24, 25]. The latest soot models include detailed gas phase reaction kinetics and specifically defined elementary processes leading to soot nucleation, mass and size growth, and oxidation. Advanced and fast numerical techniques are also available to solve the dynamics of soot formation and provide the evolution of soot PSDs [25].

To this date most of the modelling work has concentrated on matching the numerical results with mean properties of soot PSDs, including soot volume fraction and total number density. These studies have led to a wide range of basic understanding concerning the chemistry and physics of soot formation, but many questions remain and debate continues. These questions include, for example, the nature and size of soot nuclei, the mechanism of soot inception, the nature and number of chemically active sites on soot surface available for gas-surface reaction, and the sticking probabilities of particle-particle and PAH-particle collision. Over the last decade, progresses have been somewhat limited partly because a further understanding of these issues requires experimental information about soot PSDs beyond their mean properties.

The recent developments of advanced soot measurement techniques, including the probe sampling followed by detailed PSD measurements with a Scanning Mobility Particle Sizer (SMPS) [3, 4, 5, 6], Small Angle X-ray Scattering [7] and Small Angle Neutron Scattering [8] have provided soot data beyond the mean properties of PSDs. The spatial and temporal evolution of soot PSDs resulting from these experimental developments offer some unique modelling opportunities and challenges. The various issues concerning soot inception and mass growth may now be investigated on the basis of the new and more detailed experimental data and the recent development of advanced numerical techniques for solving the dynamics of soot formation [25, 26, 27, 28].

To isolate various issues concerning soot inception and mass growth one is interested in investigating the spatial and temporal evolution of the soot particle size distribution in simple systems, e.g., laminar premixed flames. In a recent study, Zhao et al. [6] presented experimental data on the variations of soot particle size distributions as a function of the maximum flame temperature. These measurements were obtained for a series of burner-stabilized, laminar, premixed ethylene-oxygen-argon flames at a pressure of 1 bar. The purpose of this paper is to present an attempt at modelling these PSDs and test the sensitivity of soot PSDs with respect to processes and parameters in the soot model. This information will help to provide insights

to further our understanding of the fundamental sooting processes and to refine available models of soot formation.

The base soot model used in the current study was based on that documented in Appel et al. [13], which has been widely used in recent years. The gas-phase chemistry of this model is largely based on that of Wang and Frenklach [11] for PAH formation in C_2 hydrocarbon flames; the particle inception and growth kinetics and mechanism derive from the early work of Frenklach and Wang [9]. The computational method used to obtain soot PSD is the stochastic approach [25, 26, 27, 28] which gives the exact solution to the population balance equation describing the dynamics of the particle population.

The paper is organized in the following manner. In section 2 the experimental data of [6] are discussed in detail and the points for comparison of soot PSDs are outlined. The results obtained from the soot model are then compared to the experimental measurements. In section 3 we discuss the computational details. In section 4 and 5 computational results are compared to the experimental data and numerical sensitivity studies are performed to understand the effect of model parameters on the soot PSDs. Also, inferences are drawn from these analysis and potential improvements are proposed to resolve the model and experimental discrepancies.

2 Experimental Data Analysis

The ethylene-oxygen-diluent flames in [6], described in **Table 1**, were chosen for the current study. In unburned gas the fuel and oxygen composition was held fixed (24.2%-mol C_2H_4 and 37.9%-mol O_2), but maximum flame temperature differ due to variations of cold gas velocity (series A) or the inert composition (series B). The two sets of flames were designed to provide conditions leading to both unimodal and bimodal PSDs within the measurable range of particle diameters by SMPS.

Table 1: *Summary of flame conditions.*

Flame code	Mol% diluent Ar/N_2 [a]	Cold gas vel. (cm/s)	T_{max} (K)	PSD characteristics for $H = 7/10$ mm[b]			
				$D_{p,a}$ (nm)[c]	nnd_a	$D_{p,b}$ (nm)	$D_{p,c}$ (nm)
A1	37.9/0	7.0	1790	4.3/4.1	1.0/0.13	8/14	17/41
A2	37.9/0	7.85	1820	3.3/3.2	0.6/0.08	6/11	15/32
A3	37.9/0	10.0	1920	–/–	–/–	5/6	10/17
B1	0/37.9	8.0	1790	4.2/3.6	1.1/0.15	7/13	15/42
B2	15.1/22.8	8.0	1810	–/2.9	–/0.14	5/10	10/24
B3	37.9/0	8.0	1840	–/–	–/–	6/9	13/26

[a] Unburned gas contains 24.2%-mol C_2H_4 and 37.9%-mol O_2.
[b] See **Fig. 1** H is the distance from the burner surface. [c] Accurate to within 0.5nm.

The PSDs were measured as a function of distance H from the burner surface and usually cover the range of $H = 5$ to 12 mm. In [6] the SMPS mobility diameter was

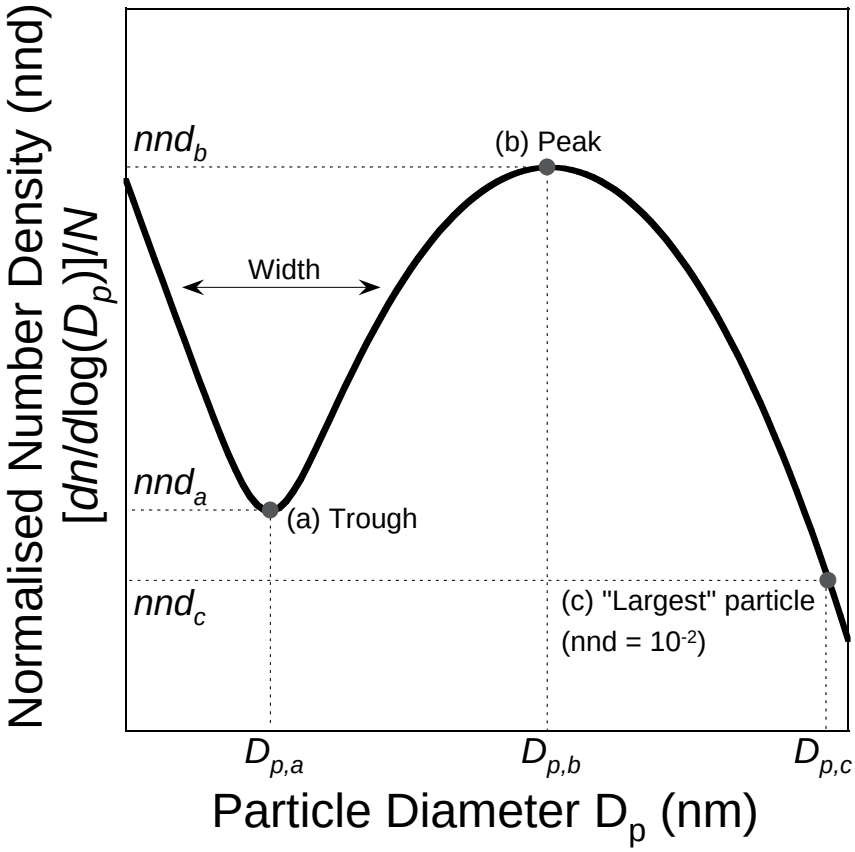

Figure 1: *Characteristic particle diameters and their corresponding normalized number densities.*

corrected to yield real diameter on the basis of a nanoparticle transport theory developed recently [29, 30], which supersedes the Stocks-Cunningham formula of electric mobility. More recent studies [31, 32] show that the momentum accommodation function of the aforementioned theory must depend critically on the particle material and that the change from specular-to-diffusion scattering occurs somewhat slower for carbon-like material than for silver or copper oxide data analyzed in [30]. As a result, a new correlation between real and mobility particle diameter for spherical carbonaceous particles is proposed here as

$$\frac{D_p}{D_{p,SMPS}} = \tanh(1.3582 + 0.0122\ D_{p,SMPS}) - 0.42877\ D_{p,SMPS} \qquad (1)$$

for air at room temperatures and $2\,\text{nm} < D_{p,SMPS} < 100$ nm. In the above equation, $D_{p,SMPS}$ is the mobility diameter (nm) directly measured by SMPS. This correlation replaces the one presented in Fig. 2 of [6]. The PSDs of the current paper are calculated from the SMPS mobility diameter using the above correlation. The changes in the revised experimental PSDs are insignificant compared to those shown in [6].

The basic hypothesis of [6] is that the feature of PSD, and especially the bimodality observed earlier [5], is strongly dependent on temperature, which in turn determines

whether the PSD is bimodal or unimodal within the particle size range detectable by SMPS. Low temperature flames tend to produce bimodal PSD because of persistent particle inception and the competition between particle inception and particle-particle coagulation [5]. For high temperature flames, the thermal dissociation of PAHs becomes significant in the post flames. This effectively stops the particle inception process and eliminates the competition between inception and coagulation. As a result, the PSDs tend to be unimodal.

For flames where bimodal distributions are observed, the evolution of PSDs may be characterized by an initial, power-law type PSD for incipient soot, which evolves into a bimodal PSD upon particle size and mass growth. The second PSD is of log-normal type, whereas the first PSD remains to be a power-law function. The basic features of measured bimodal PSDs are schematically shown in **Fig. 1**. For the purpose of comparing PSDs, three characteristic points on a PSD may be identified as (a) the trough applicable to bimodal PSDs only, (b) the "maximum", normalized number density nnd, and (c) the "largest" detected particle diameter, conveniently defined here as the greatest diameter for which $nnd = 10^{-2}$. Each of these features may be quantified by their corresponding particle diameter and nnd values. For example, $D_{p,a}$ and nnd_a denote the diameter and normalized number density at the bottom of the bimodal PSD trough, as seen in Fig. 1.

The following observations apply to all bimodal PSDs. The size of the smallest soot particle obtained from the SMPS measurement is 2.5 nm. Smaller particles obviously exist in the flame, but they were not detected because of the instrument limitation. The diameters at points (b) and (c), see Fig. 1 and Table 1, both increase with H. The diameter $D_{p,a}$ remains almost constant for a flame. However, its nnd decreases as H increases. Not all features are common to all the flames. Therefore, the flames were also analyzed for variations with the flame conditions. The PSDs for Flames A1 and B1 are bimodal, whereas Flames A3 and B3 have unimodal PSDs. Flames A2 and B2 are intermediate cases with one of the two modes less significant. The flames with higher peak temperatures (A3 and B3) give unimodal PSDs and have $D_{p,c}$ values smaller than those of other flames, as seen in Table 1.

3 Numerical Details

A detailed kinetic model of soot formation, from the perspective of computer implementation, can be considered to consist of two principal components: gas phase chemistry, which determines the flame structure and soot population dynamics, which describes the evolution of the particle ensemble. In this work, the flame chemistry and PAH formation and growth were computed using the reaction model of [13], termed ABF for this paper. It is important to mention that the accuracy of the particle dynamics submodel relies on the accuracy of the species profiles supplied by the gas phase model. The ABF gas phase model represented several important revisions to that of [11] and predicts pyrene and acetylene concentrations, which are important gas species to predict soot PSD, better than the original model. The

flame structure was then calculated employing a modified version of the PREMIX code [33, 34], using the measured temperature profile. The code also solves the transport equations of the moments of the size distribution of soot particles applying the detailed soot model to be described below. In this manner, formation and consumption of gas phase species due to soot formation and oxidation were approximately accounted for.

The predicted species profiles were used as input to the stochastic simulation [27, 28]. The stochastic code solves the soot population balance equation, accounts for gas expansion due to temperature variation within the flame, and obtains fully resolved soot particle size distributions. The soot submodel contains three principal processes. Particle inception is assumed to occur through collision and coalescence of two pyrene molecules [13]. Coagulation and coalescence of soot particles give larger soot particle. Surface processes include the reactions of gaseous C_2H_2, O_2 and OH with soot surface and pyrene condensation. The fraction of active sites on the soot surface α, modelled by a general fit to eight laminar premixed flames [13], was used here initially without modification.

4 Numerical Results

Before comparing the simulation results of soot PSDs with the experimental observations, we want to allow for effects of probe perturbation. Such effects arise primarily from flame cooling by the probe and changes of gas velocity and thus the particle time history within the flame [4]. This will also account for particle-particle coagulation in the sample probe, even though experimental evidence shows that this coagulation to be insignificant [6]. These effects usually result in a need to spatially shift the numerical results to achieve proper comparison between model and experiment. We first examined soot PSDs of Flames A3 and B3. These two flames were chosen as they are most likely to match the experimental observations, considering that they have unimodal distribution and thus smaller numbers of PSD parameters to be compared. Also, the higher peak temperatures of these two flames and smaller measured particle size suggest little to no soot aggregation. This is in line with the assumption of spherical soot particles in the current model.

For Flame B3, the experimental data and two sets of simulation data are plotted in **Fig. 2**. For proper comparison with the experimental data, the simulated number density is normalized by the total number density of particles with $D_p > 2.5$ nm. The resulting simulated *nnd*'s are represented by the dashed lines without height offset, whereas the solid lines were shifted by -3.5 mm to match the PSD profile at $H = 5$ mm. It is seen that the numerical results match the measurements very well upon this height offset. It was observed that the offset appear to be proportional to the inlet velocity of the unburnt gas mixture. Therefore, an offset of 4 mm for Flame A3 and 3.25 mm for Flame A1 was used, again, by matching the PSD profile at $H = 5$ mm. The comparisons are illustrated in **Figs. 3 and 4**, where only shifted numerical *nnd*'s are shown.

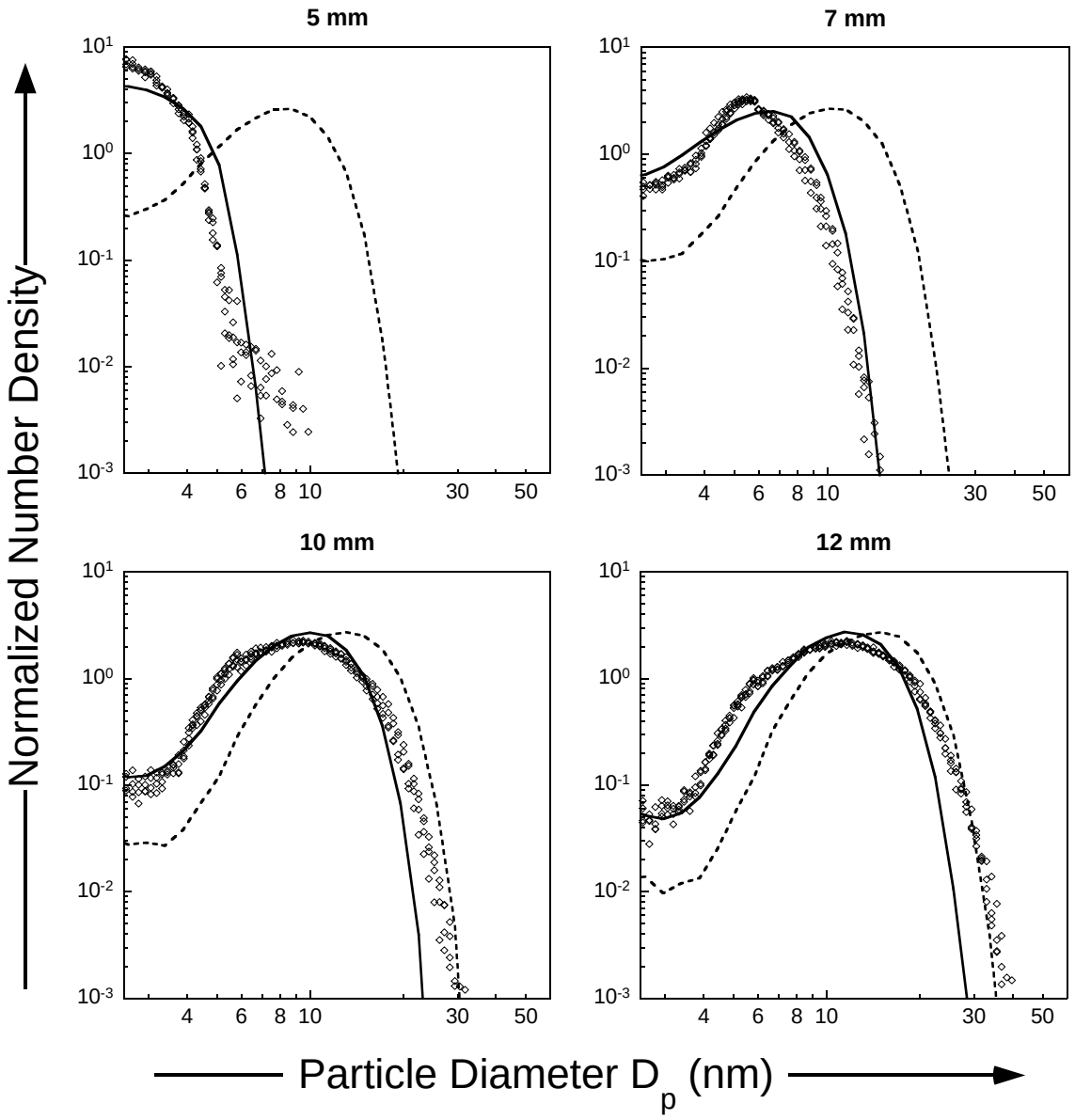

Figure 2: *Normalized number density distribution of Flame B3. The symbols represent the experimental measurements at distance H mm, (- - -) represents numerical result as is without height offset, and (—) represents numerical results at $H - 3.5$ mm.*

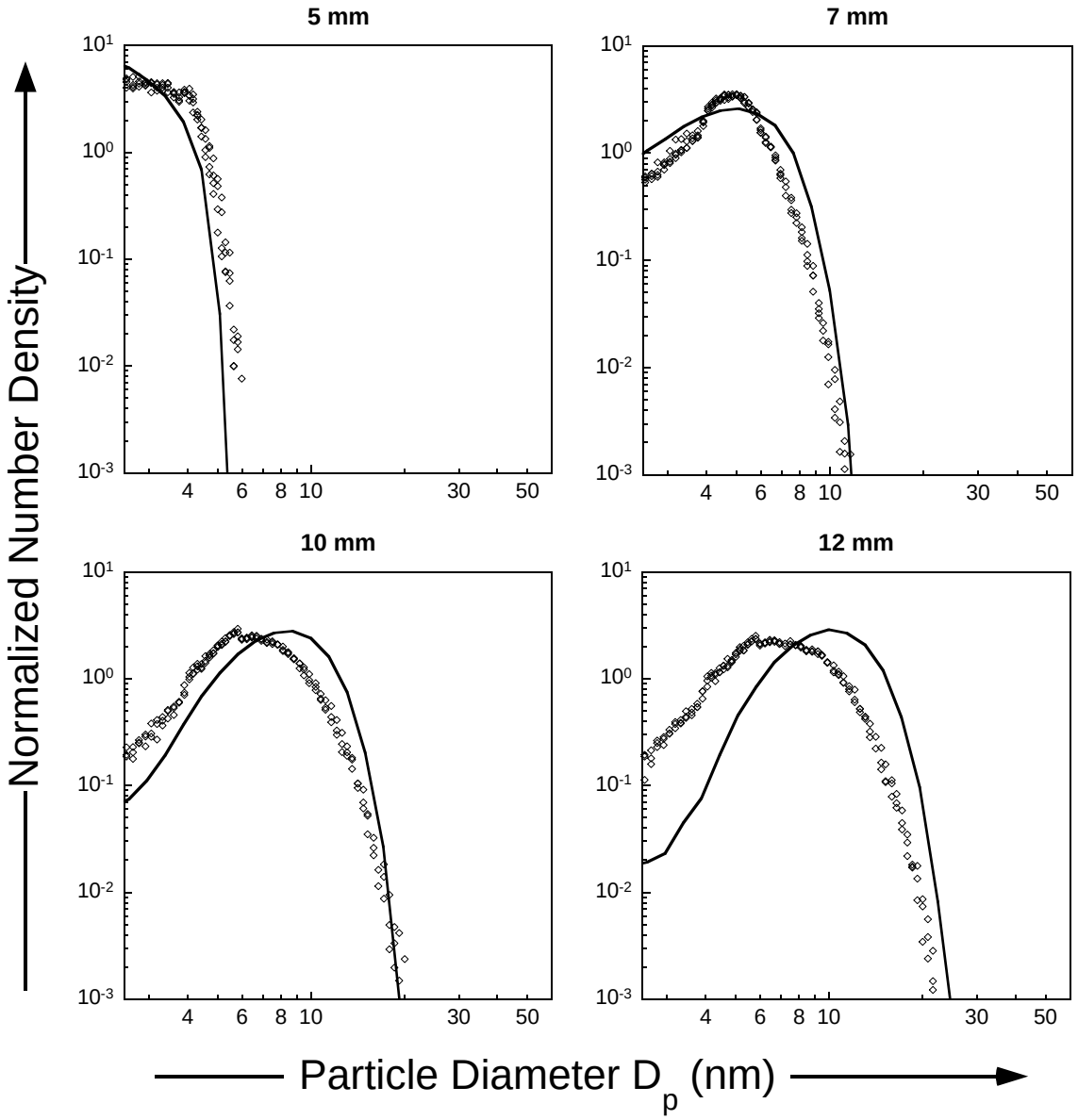

Figure 3: *Normalized number density distribution of Flame A3. The symbols represent the experimental measurements at distance H mm, and (—) represents numerical results at $H - 4$ mm.*

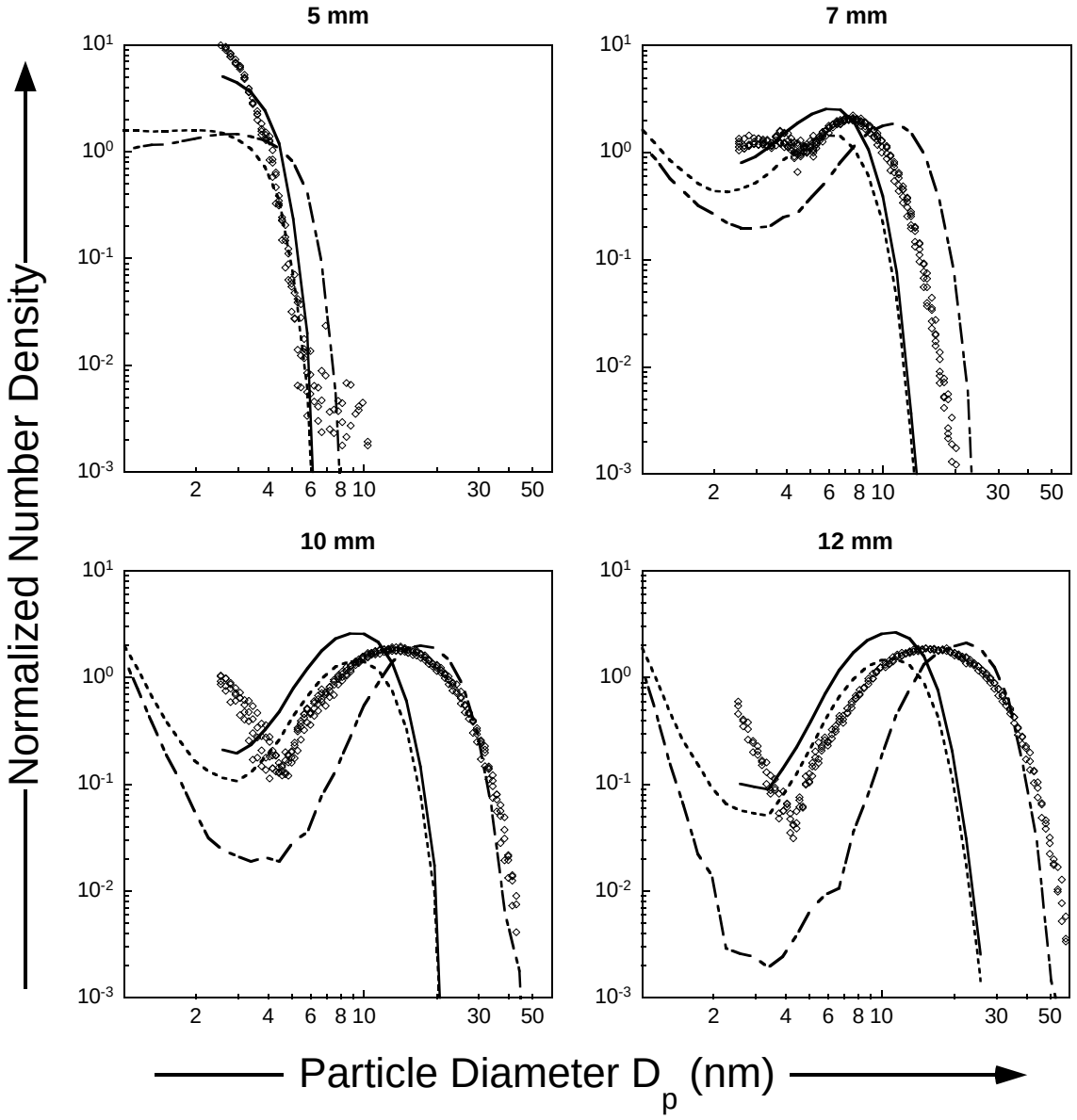

Figure 4: *Normalized number density distribution of Flame A1. The symbols represent the experimental measurements at distance H mm, and lines represents numerical results at $H - 3.25$ mm: (—) PSD normalization uses the total number density N for particles with $D_p > 2.5$ nm, (- - -) normalization uses N for $D_p > 0.9$ nm, and (– - –) increased the fraction of active surface site density by 30%.*

As seen in Figs. 2 through 4, reasonably good agreements were observed between the experimental measurements and simulations, especially at smaller distances from the burner surface. For Flames A2, B1 and B2, the results are comparable to those presented in Figs. 2 through 4. In this regard, the computational results are encouraging considering that with only a spatial shift the evolution of the PSDs computed for each flame can be plotted on the same plot as the experimental data without having to invoking model parameter adjustments. As can be seen from these figures, unimodal distributions can be predicted to fairly good accuracy. The real challange, however, lies in predicting bimodal distribution because there are more parameters to be matched than in the unimodal distribution. Therefore, the Flame A1 will form the major part of the remaining discussion.

For large H values of Flame A1, the model under predicts the particle diameter. One explanation for this difference is the absence of accurate models for the surface processes. This problem will be studied in detail later in the paper. It is also observed in Fig. 4 that the bimodality of Flame A1 and its development are qualitatively well predicted (*cf*, experimental data and the dashed lines), but the bottom of the PSD trough occurs at particle diameter smaller than the observed size. The simulated $D_{p,a}$ (defined in Fig. 1) is 3 nm and about 1.5 nm smaller than that in the experimental observations. Likewise, the $D_{p,b}$ and $D_{p,c}$ values are both under predicted.

5 Numerical Sensitivity Analysis

Drawing motivation from the discrepancies between simulated and observed PSDs shown in Fig. 4 and considering the nonlinear response of the PSD characteristics with respect to the model parameters, numerical experiments were performed to identify parameters of the soot model that affect the detailed PSD features. The model parameters considered here include the size of the "smallest" particle $N_{c,0}$, i.e., 32 carbon atoms in the base case due to assumption of pyrene-pyrene coalescence, the sticking probability of PAH-PAH (pyrene) collision ($\gamma_{PAH-PAH}$), the sticking probability of PAH-particle collision (γ_{PAH-P}), the average Van der Waal's enhancement factor $\varepsilon = 2.2$, and the active surface site density α as defined in [13]. Unless otherwise indicated, the base case numerical experiment mentioned henceforth uses the soot model [13] unaltered. A new description of the surface active sites, proposed more recently in [26], is employed occasionally and its use will be specifically indicated.

5.1 Sticking Probability of Pyrene-Pyrene Collision

Binary collisions between PAH molecules to give a dimer have been an area of investigation [35]. The understanding that the dimer might not be stabilized on time before it reverts to two pyrene molecules have led us to examine the influence of

non-unity sticking probability on the predicted PSDs. In **Fig. 5**, we observe that the gas-phase pyrene concentration increases as we decrease the sticking probability $\gamma_{PAH-PAH}$. It is noteworthy that for $H > 2-3$ mm the drop in the pyrene concentration from $\gamma_{PAH-PAH} = 0$ (no inception) to 10^{-4} is caused by a combination of little inception and a lot of pyrene condensation on soot particles.

In **Fig. 6**, we compare the PSDs resulting from different $\gamma_{PAH-PAH}$ values. Qualitatively, it can be seen that with the decrease in $\gamma_{PAH-PAH}$, the PSD trough shifts to smaller soot particle sizes. Quantitatively, this shift and the nnd_a is not commensurate to the shift in magnitude of $\gamma_{PAH-PAH}$. We observed similar trends for Flame B1, which also has a bimodal distribution. It is also possible to consider an increased collision cross section of pyrene-pyrene molecules due to Van der Waals interactions [36]. However, looking at results shown in Fig. 6, one can infer that this would not make much difference to the PSD, because this enhancement factor is relatively small.

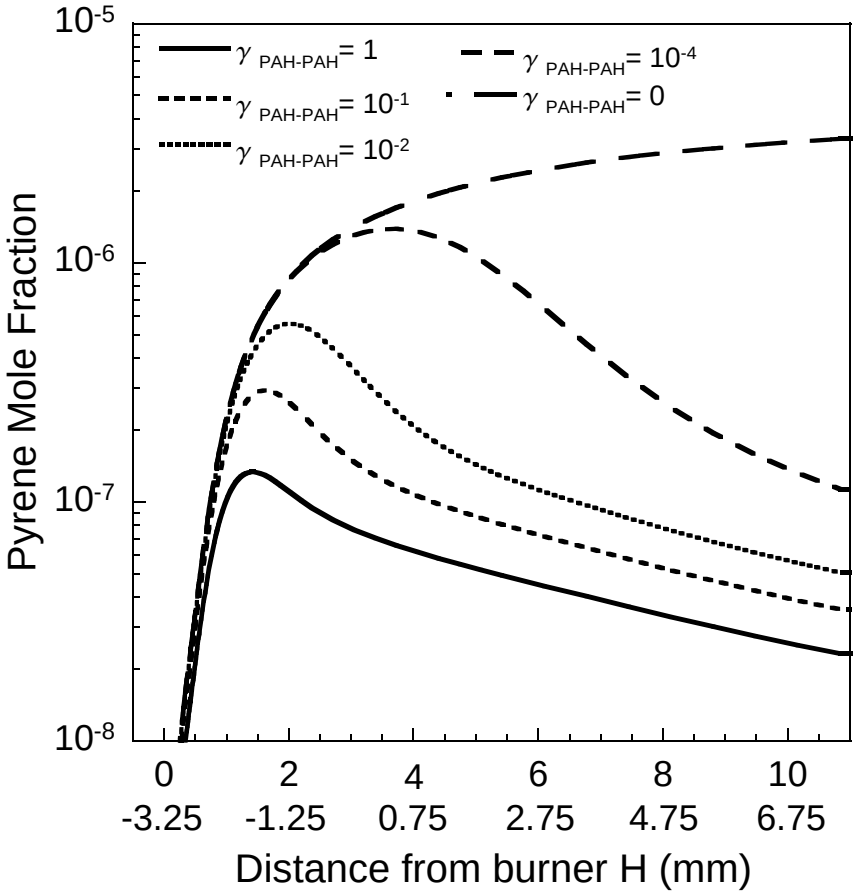

Figure 5: *Sensitivity of pyrene mole fraction profile with respect to the pyrene-pyrene sticking probability $\gamma_{PAH-PAH}$ computed for Flame A1. Secondary X axis is the spatially shifted distance.*

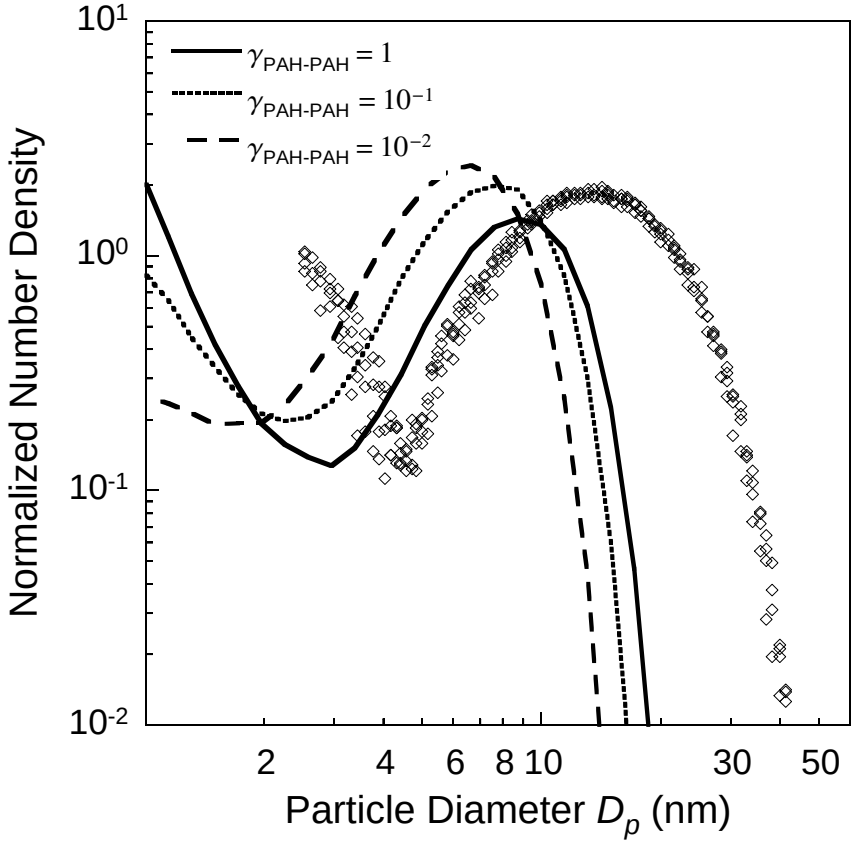

Figure 6: *Sensitivity of PSD ($H = 10$ mm, Flame A1) with respect to $\gamma_{PAH-PAH}$.*

5.2 Sticking Probability of PAH-Particle Collision

We can observe from **Fig. 7** that the gas-phase pyrene concentration increases substantially with a decrease in the sticking probability of PAH-particle collisions γ_{PAH-p}. The reduced γ_{PAH-p} values hardly affect $D_{p,b}$, but they shift the bottom of the trough towards larger size with lower corresponding *nnd*, as seen in **Fig. 8**. The computed $D_{p,a}$ value is sensitive to the PAH condensation rate but not to the rate of particle inception due to dimerization. However, to increase computed $D_{p,a}$ and resolving the differences in computational and experimental PSDs (see, Fig. 4), the corresponding change in γ_{PAH-p} may be difficult to justify physically, especially considering that $\gamma_{PAH-PAH}$ is expected to be smaller than γ_{PAH-p} and a reduced γ_{PAH-p} would suggest a further reduced $\gamma_{PAH-PAH}$. The latter would lead to a decrease in $D_{p,a}$ (see, **Fig. 6**) and thus it has a compensating effect to the decrease in γ_{PAH-p}.

5.3 Density of Active Surface Sites

Numerous sets of reaction mechanisms and kinetic parameters have been proposed for soot surface growth [9, 13, 20], illustrating the fact that the exact surface growth

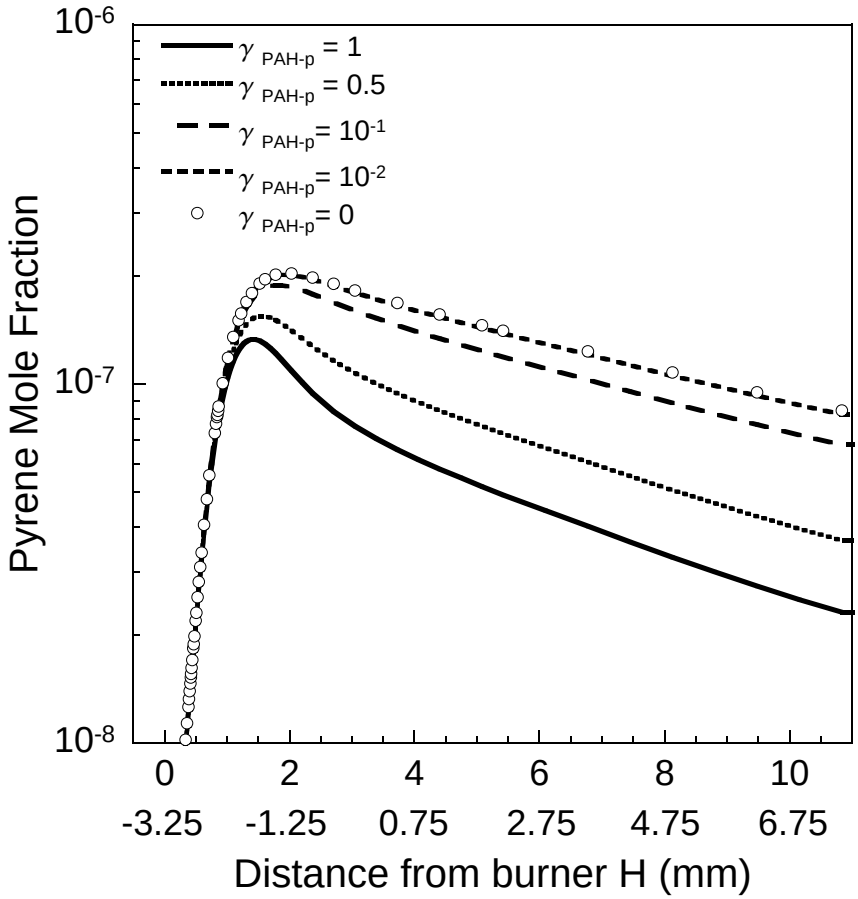

Figure 7: *Sensitivity of pyrene mole fraction profile with respect to the γ_{PAH-p} computed for Flame A1. Secondary X axis is the spatially shifted distance.*

kinetics is far from being understood. A recent photoionization aerosol mass spectrometry study [37] on a similar ethylene flame showed that in the late stage of their mass growth soot particles contain a large amount of aliphatics. Depending on the equivalence ratio and possibly temperature, the aliphatic content can be as large as the aromatic content. The mass growth through the reaction of soot with aliphatics is not accounted for in the current soot model. Hence, the under-prediction of particle size and especially in the log-normal part of the PSDs of large H values (see, Fig. 4) may be the consequence of inaccurate surface reaction rate as well as the lack of appropriate mass growth paths.

In this study, the numerical sensitivity analysis is carried out by uniformly increasing the fraction of active sites on the surface of the soot particles α (i.e., Eq. (1) of [13])– one of the most empirical parameters in the soot model-by 30%. This effectively increases the overall surface reaction rate by the same percentage value, without an explicit indication, for the time being, of the mechanism by which such an increase may be justified. Because within the framework of the current soot model acetylene addition is responsible for most of the mass added into the system, the

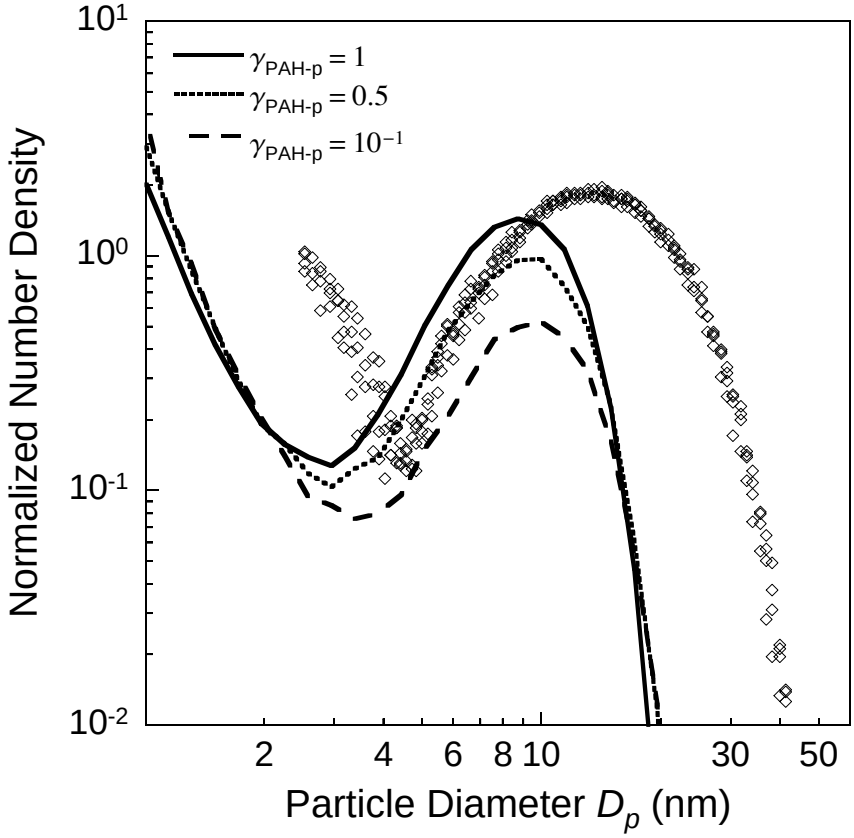

Figure 8: *Sensitivity of PSD ($H = 10$ mm, Flame A1) with respect to γ_{PAH-p}.*

impact of this parameter was expected to be significant on the soot PSD. Indeed, we observe, from Fig. 4 (dash-dotted-dash line), that all characteristic particle diameters, i.e., $D_{p,a}$, $D_{p,b}$ and $D_{p,c}$, becomes uniformly and notably larger for all H values. For large H values, the shift of the simulated PSDs to larger particle sizes would appear to provide better agreement between experimental and simulated PSD profiles. Yet one cannot conclude that the increase in the surface reactivity is, even partially, a solution to the problem. Recall that the simulated PSD profiles were spatially shifted to compensate for the probe effects. Since the amount of such shift is empirical, the increase of particle sizes, brought by an increased α, can be compensated by adjusting the spatial shift of the computed profiles. Meanwhile, the trough in bimodal PSDs deepens significantly, and it becomes too deep as compared to the observed PSDs, especially for large H values. In addition, a uniform increase of surface reactivity does not broaden the log-normal part of the PSDs sufficiently to match the experimental profiles.

As suggested by a referee of [26] we propose that the number of active sites on an individual particle is a function of the local flame temperature and its residence time in the flame. Mathematically, for each particle

$$\frac{\mathrm{d}}{\mathrm{d}t} s_a(t) = -C\ T(t)\ [s_a(t) - s_{base}], \quad s_a(0) = 2.3 \times 10^{15}\ \mathrm{cm}^{-2} \tag{2}$$

where we assume that the number of active sites never becomes zero and use $s_{base} = 4.6 \times 10^{14}$ cm^{-2} and $C = 0.1$ motivated from [26].

Upon coalescence of two soot particles, the density of active sites on the new soot particle is set to the surface area weighted mean of the densities for the coalescing particles. Here, the use of local temperature provides a more realistic and physically motivated description for the particle ageing. This is still a simplistic model, but the prediction appears to be improved over the original, base soot model where only the maximum flame temperature is used in the equation of active surface density [13]. A comparison of the two surface site models is presented in **Fig. 9**. Though the prediction with equation 2 is far from being perfect, the spacing between the bottom of the PSD trough and the diameter of PSD peak, $D_p, b - D_p, a$, is much better predicted. For the remaining studies, the base case will include the above surface ageing model.

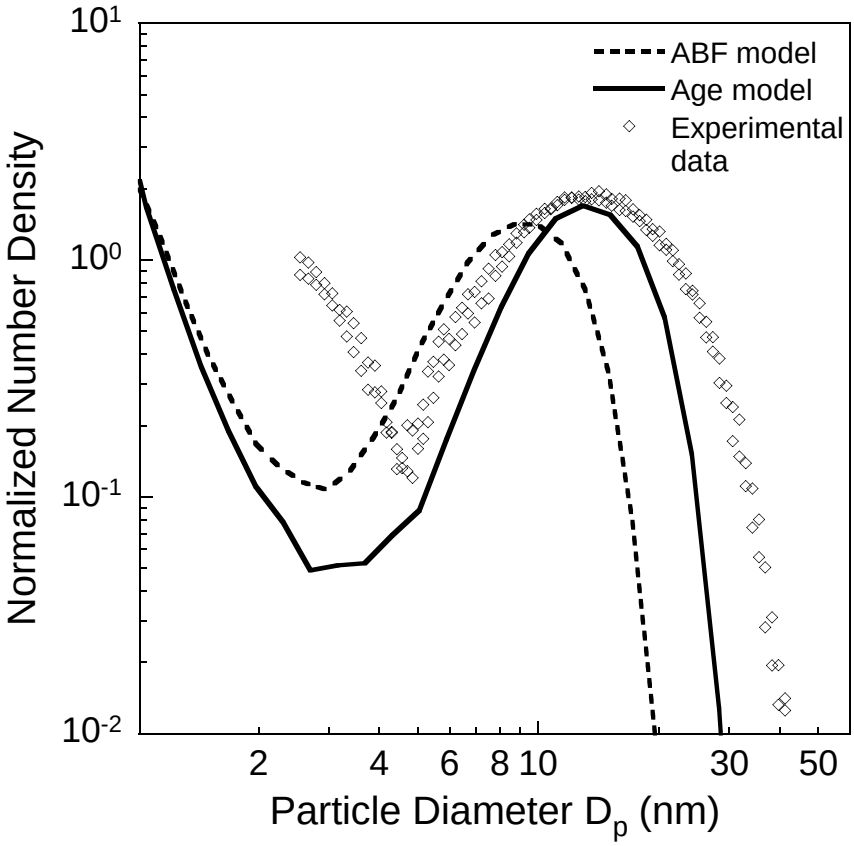

Figure 9: *Sensitivity of PSD ($H = 10$ mm, Flame A1) with respect to the surface site model.*

5.4 Assumption of "Smallest" Model Particle

Prior to the work of [38], particle inception was generally assumed to involve the dimerization of PAHs (>= pyrene) of different sizes. This may be implemented in

soot models with a linear lumping algorithm [9]. Various groups have also adopted inception models to include PAH growth beyond pyrene [14, 20, 16, 39]. It was shown in [38] that from the standpoint of predictions of mean particle properties, *e.g.*, volume fraction, this assumption yields practically the same result as assuming pyrene dimerization as the only step of particle inception. To predict the detailed soot PSDs, however, particle inception from pyrene dimerisation only may not be adequate because the position of the PSD trough can be very sensitive to the size of the first particle. Therefore, the inception model is examined here by increasing the size of the first soot particle to 224 carbon atoms from 32 atoms [1]. These large soot particles could be formed by dimerisation of higher PAHs or coalescence of higher and lower PAHs.

The study was divided into two sections: (a) only the size of the first particle was increased to 224 carbon atoms without changing the particle inception rate, and (b) the inception rate for case (a) was reduced by a factor of 7 to ensure that the amount of carbon added into the system was equal to that in the base case. We observe from the **Fig. 10** that case (a) shifts the bottom of the trough significantly to larger size with higher corresponding nnd_a than the base case, and case (b) shifts the position of minima significantly to smaller soot particle size, but with even higher corresponding nnd_a.

It is generally true that with each addition of an aromatic ring, the concentration of PAHs decreases by about one order of magnitude [40]. One might therefore expect that the concentration of higher PAHs, such as the ones containing 112 carbon atoms, to be considerably lower than the concentration of pyrene. Thus, a significantly lower inception rate would be expected from higher PAHs as compared to pyrene. However, it is important to keep in mind that most of the pyrene in the base case is consumed in pyrene condensation. The typical utilization ratio of pyrene in condensation to inception is 10 to 1 for bimodal flames and 1000 to 1 for unimodal flames. This implies that one could achieve similar amounts of particle inception with an order or two orders of magnitude lower concentration of pyrene if the condensation process was not occurring. Therefore, if we assume that the higher PAHs are not involved in condensation in the same way as the smaller PAHs, it is possible to envisage similar inception rates as are obtained in the base case.

In summary, the assumption about the first particle size coupled with particle inception rate has large effects on the predicted soot PSD. To account for details of soot PSDs in these flames, a detailed chemistry model is therefore preferable, where a mixture of small and large PAHs should be considered in soot inception. Analysis of the path of formation for pyrene and higher PAHs is not within the scope of this paper.

[1] Soot particles containing 224 carbon atoms correspond to spherical particles of diameter 1.68 nm, which is below the detection limit of the SMPS

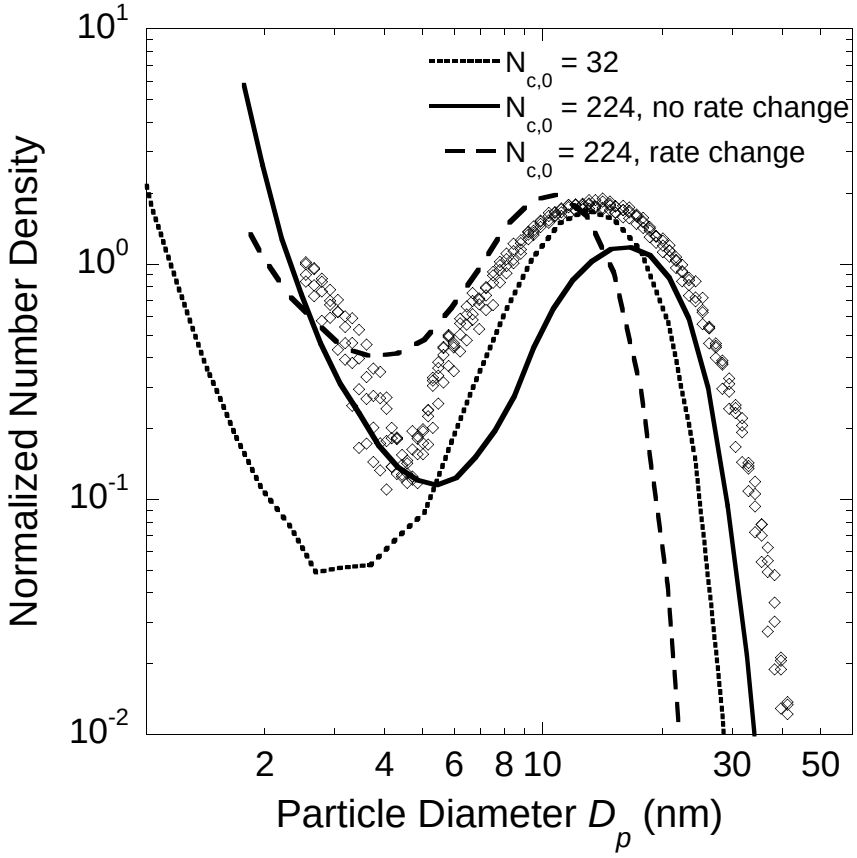

Figure 10: *Sensitivity of PSD ($H = 10$ mm, Flame A1) with respect to size of the smallest soot particle $N_{c,0}$ and nucleation rate.*

5.5 Particle-Particle Coagulation: Effect of Van der Waals Enhancement Factors

For the current flames, where most of the particle interactions occur in the free molecular regime, the probability of small and large soot particles coagulating is much larger than that of small-small or large-large coagulations. The differential collision kernels, therefore, must exert an effect on particle size distribution. Though these kernels are exactly implemented in the soot model, the van der Waals enhancement factor was assumed to be a constant (2.2), an average over the range of soot particle sizes [36]. The enhancement factors for small-large soot particles coagulating vary between 1.2 and 1.8, which is well below the average value of 2.2. For this reason, we tested the effect of a particle-size dependent enhancement factor on the soot PSDs. It can be observed from the **Fig.11** that the position of the PSD trough shifts towards larger sizes with a higher corresponding nnd_a when the more detailed enhancement factors are used. This is because less of smaller particles are being absorbed by the large particles, increasing their relative number density compared to the base case. The post minima distribution is not significantly affected.

The qualitative effects of the parameters of the soot model on soot PSD is summa-

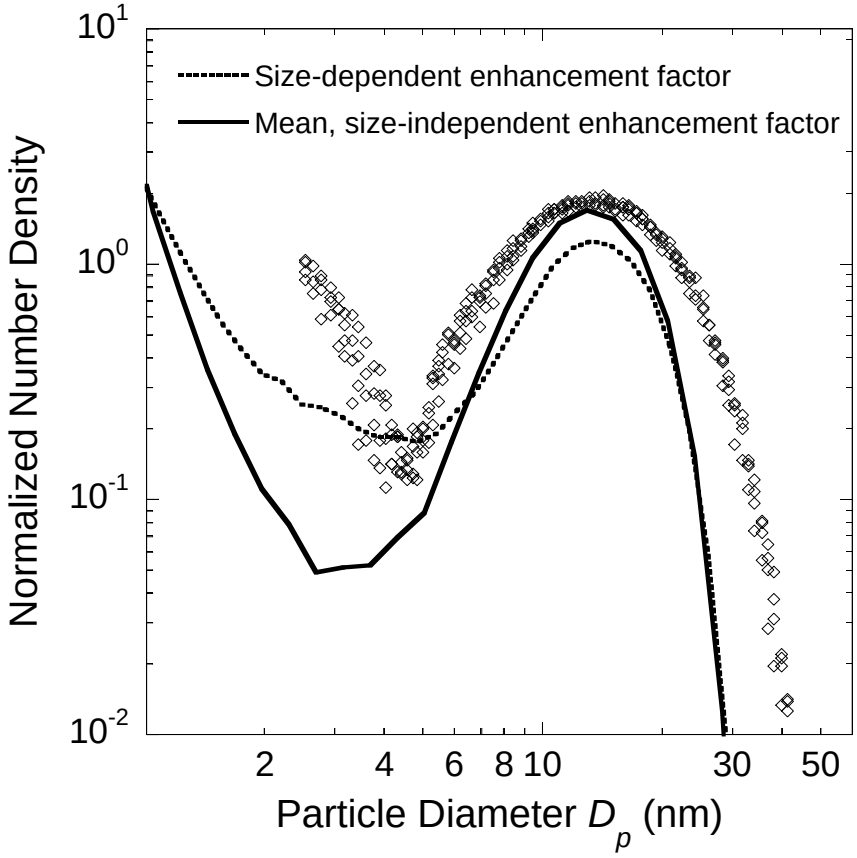

Figure 11: *Sensitivity of PSD (H = 10 mm, Flame A1) with respect to size-dependent enhancement factor.*

rized in **Fig. 12**. It is clear that a closer prediction of the experimental PSDs may be brought by an increase in the size of nucleating PAHs coupled with a somewhat reduced particle inception rate, an increase in the surface growth rates, and/or the use of a size dependent van der Waals enhancement factor and a consideration of the sticking probability for particle-particle coagulation. These parameters might have to be varied in different quantities for different flames. The scope of the paper and the various coupled experimental and model uncertainties do not allow to establish a fixed numerical value for these parameters at this, but the work establishes the baseline of comparison between experimental and simulated soot PSDs and their evolution. It also provides insights into the qualitative and quantitative behaviors of soot PSDs with respect to a large number of model parameters.

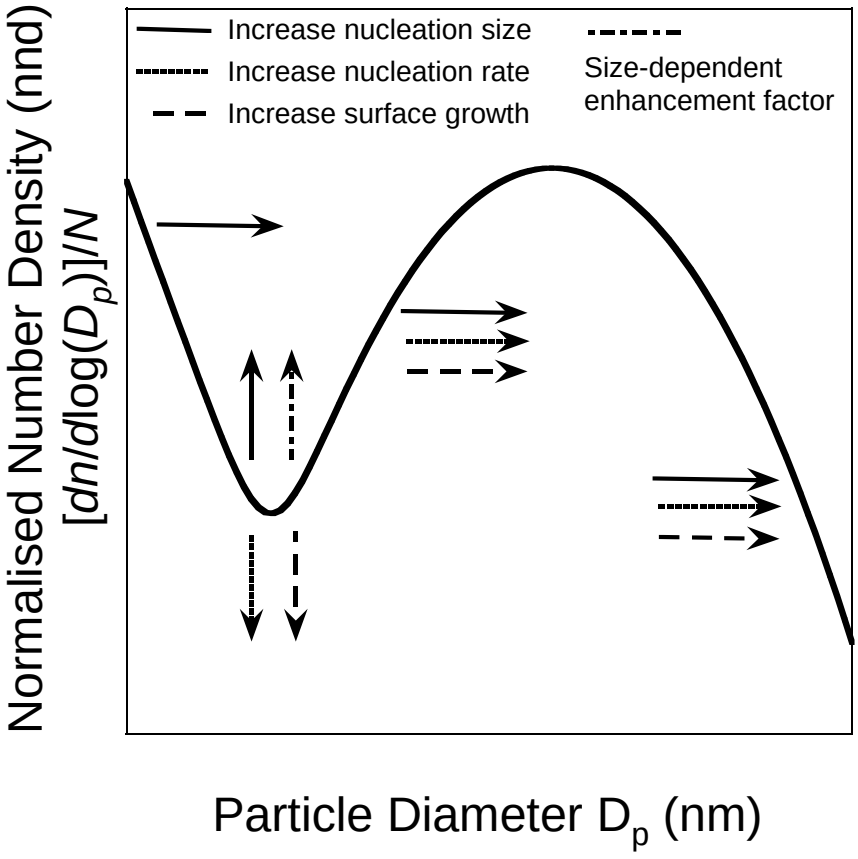

Figure 12: *Summary of effects of parameters of soot model on soot PSD.*

6 Conclusion

For the first time, the ability of the soot model presented in Appel et al. [13] to predict the evolution of detailed soot PSDs is tested by comparing simulated results with experimental observations of soot PSDs. A stochastic particle method was used to obtain particle size distributions. The key features of the measured and simulated particle size distributions were identified and used as a simple way of comparing PSDs. The sensitivity of the soot PSD to the processes and parameters defining the ABF soot model, such as the soot inception model, van der Waals enhancement of particle-particle coagulation, and surface activity model was investigated.

An increase in the incepting particle size was shown to have a very significant effect on the lower end of the PSDs, especially the trough of a bimodal PSD. This, while known, was quantified by estimating the size of poly aromatic hydrocarbons used in the inception process. This result suggests that to predict the details of soot PSDs and their evolution the chemistry for higher PAHs and a more elaborate inception model are needed where PAHs interact to give incepting soot particles of varied sizes.

A new model for the decay in the surface activity, proposed recently [28], in which the activity of the soot particle depends only on the history of that particle and the local temperature of the flame, is shown to provide better predictions for soot PSDs than a previous surface ageing model in which the surface active sites are assumed to depend on the maximum flame temperature only. This new model is still too simplistic and should incorporate soot surface interactions with the surrounding gaseous species.

The paper has contributed in quantifying the sensitivities of soot PSD to parameters of the soot model and provided insight into future developments.

Acknowledgements

The support of JS, RIAP, and MK by Trinity and Churchill College, Cambridge, and the EPSRC (Grant number GR/R85662/01) is gratefully acknowledged. The work at USC was supported by the National Science Foundation CHE-0089136.

References

[1] H. Bockhorn, F. Fetting, A. Heddrich, and G. Wannemacher. Investigation of the surface growth of soot in flat low pressure hydrocarbon oxygen flames. *Proceedings of the Combustion Institute*, 20:979–988, 1984.

[2] F. Xu, P. B. Sunderland, and G. M. Faeth. Soot formation in laminar premixed ethylene/air flames at atmospheric pressure. *Combustion and Flame*, 108:471–493, 1997.

[3] Maricq M. Size and charge of soot particle in rich premixed ethylene flames. *Combustion and Flame*, 137:340–350, 2004.

[4] B. Zhao, Z. Yang, J. Wang, M. V. Johnston, and H. Wang. Analysis of soot nanoparticles in a laminar premixed ethylene flame by scanning mobility particle sizer. *Aerosol Science and Technology*, 37:611–620, 2003.

[5] B. Zhao, Z. Yang, M. V. Johnston, H. Wang, A. S. Wexler, M. Balthasar, and M. Kraft. Measurement and numerical simulation of soot particle size distribution function in a laminar premixed ethylene-oxygen-argon flame. *Combustion and Flame*, 133:173–188, 2003.

[6] B. Zhao, Z. Yang, Z. Li, M. V. Johnston, and H. Wang. Particle size distribution function of incipient soot in laminar premixed ethylene flames: Effect of flame temperature. *Proceedings of the Combustion Institute*, 30:1441–1448, 2005.

[7] J. P. Hessler, S. Seifert, and R. E. Winans. Spatially resolved small-angle x-ray scattering studies of soot inception and growth. *Proceedings of the Combustion Institute*, 29:2743–2748, 2002.

[8] H. Wang, B. Zhao, B. Wyslouzil, and K. Streletzky. Small-angle neutron scattering of soot formed in laminar premixed ethylene flames. *Proceedings of the Combustion Institute*, 29:2749–2758, 2002.

[9] M. Frenklach and H. Wang. Detailed mechanism and modeling of soot particle formation. *Proceedings of the Combustion Institute*, 23:1559–1566, 1991.

[10] M. Frenklach and H. Wang. Detailed mechanism and modeling of soot particle formation. In H. Bockhorn, editor, *Soot Formation in Combustion: Mechanisms and Models*, pages 165–192. Springer Verlag, 1994.

[11] H. Wang and M. Frenklach. A detailed kinetic modeling study of aromatic formtion in laminar premixed acetylene and ethylene flames. *Combustion and Flame*, 110:173–221, 1997.

[12] I. M. Kennedy. Models of soot formation and oxidation. *Prog. Energy. Combust. Sci.*, 23:95–132, 1997.

[13] J. Appel, H. Bockhorn, and M. Frenklach. Kinetic modeling of soot formation with detailed chemistry and physics: Laminar premixed flames of C_2 hydrocarbons. *Combustion and Flame*, 121:122–136, 2000.

[14] A. D'Anna, A. Violi, and A. D'Alessio. Modeling the rich combustion of aliphatic hydrocarbons. *Combustion and Flame*, 121:418–429, 2000.

[15] J. Appel, H. Bockhorn, and M. Wulkow. A detailed numerical study of the evolution of soot particle size distributions in laminar premixed flames. *Chemosphere*, 42:635–645, 2001.

[16] H. Richter, S. Granata, W. H. Green, and J. B. Howard. Detailed modeling of pah and soot formation in a laminar premixed benzene/oxygen/argon low-pressure flame. *Proceedings of the Combustion Institute*, 30:1397–1405, 2005.

[17] M. Frenklach and S.J. Harris. Aerosol dynamics modeling using the method of moments. *Journal of Colloid Interface Science*, 118:252–262, 1986.

[18] F. Gelbard and J. H. Seinfeld. Simulation of multicomponent aerosol dynamics. *Journal of Colloid Interface Science*, 78:485–501, 1980.

[19] M. B. Colket and R. J. Hall. In H. Bockhorn, editor, *Soot Formation in Combustion: Mechanisms and Models*, pages 442–468. Springer Verlag, 1994.

[20] F. Mauss, T. Schafer, and H. Bockhorn. Inception and growth of soot particles in dependence on the surrounding gas phase. *Combustion and Flame*, 99:697–705, 1994.

[21] A. Kazakov, H. Wang, and M. Frenklach. Detailed modeling of soot formation in laminar premixed ethylene flames at a pressure of 10 bar. *Combustion and Flame*, 100:111–120, 1995.

[22] M. D. Smooke, C. S. Mcenally, L. D. Pfefferle, R. J. Hall, and M. B. Colket. Computational and experimental study of soot formation in a coflow, laminar diffusion flame. *Combustion and Flame*, 117:117–139, 1999.

[23] A. Kazakov and M. Frenklach. Dynamic modeling of soot particle coagulation and aggregation: Implementation with Method of moments and application to high- pressure laminar premixed flames. *Combustion and Flame*, 114:484–501, 1998.

[24] M. Frenklach. Method of moments with interpolative closure. *Chemical Engineering Science*, 57:2229–2239, 2002.

[25] M. Balthasar and M. Kraft. A stochastic approach to calculate the particle size distribution function of soot particles in laminar premixed flame. *Combustion and Flame*, 133:289–298, 2003.

[26] J. Singh, M. Balthasar, M. Kraft, and W. Wagner. Stochastic modelling of soot particle size and age distributions in laminar premixed flames. *Proceedings of the Combustion Institute*, 30:1457–1465, 2005.

[27] R. Patterson, J. Singh, M. Balthasar, M. Kraft, and W. Wagner. The linear process deferment algorithm: A new technique for solving population balance equations. *Preprint 26: http://www.cheng.cam.ac.uk/research/groups/como/prep.listing.html*, 2005.

[28] J. Singh, R. Patterson, M. Balthasar, M. Kraft, and W. Wagner. Modelling soot particle size distribution: Dynamics of pressure regimes. *Preprint 25: http://www.cheng.cam.ac.uk/research/groups/como/prep.listing.html*, 2005.

[29] Z. Li and H. Wang. Drag force, diffusion coefficient, and electric mobility of small particles. I. theory applicable to the free-molecule regime. *Physical Review E*, 68:061206, 2003.

[30] Z. Li and H. Wang. Drag force, diffusion coefficient, and electric mobility of small particles. II. Application. *Physical Review E*, 68:061207, 2003.

[31] Z. Li and H. Wang. Gas-nanoparticle scattering: A molecular view of momentum accommodation function. *Physical Review Letters*, 95:014502, 2005.

[32] H. Wang, D. Phares, C. Campbell, and Z. Li. *Journal of Aerosol Science*, 2005.

[33] J. Kee, K. Grcar, M. D. Smooke, and J. A. Miller. PREMIX: A FORTRAN program for modelling steady laminar one-dimensional premixed flames. Technical report, SANDIA National Laboratories, 1985.

[34] R. J. Revzan, N. J. Brown, and M. Frenklach. http://www.berkeley.edu/soot/.

[35] C. A. Schuetz and M. Frenklach. Nucleation of soot: Molecular dynamics simulations of pyrene dimerization. *Proceedings of the Combustion Institute*, 29:2307–2314, 2002.

[36] S. J. Harris and I. M. Kennedy. The coagulation of soot particles with van der waals forces. *Combustion Science and Technology*, 59:443–454, 1988.

[37] B. Oktem, M. P. Tolocka, B. Zhao, H. Wang, and M. V. Johnston. Chemical species associated with the early stage of soot growth in a laminar premixed ethyleneoxygenargon flame. *Combustion and Flame*, 2005.

[38] Y. Yoshihara, A. Kazakov, H. Wang, and M. Frenklach. Reduced mechanisms of soot formation - Applications to natural gas fueled diesel combustion. *Proceedings of the Combustion Institute*, 25:941–948, 1994.

[39] P. A. Vlasov and J. Warnatz. Detailed kinetic modeling of soot formation in hydrocarbon pyrolysis behind shock waves. *Proceedings of the Combustion Institute*, 29:2335–2341, 2002.

[40] K. H. Homann. Formation of large molecules, particulates and ions in premixed hydrocarbon flames; Progress and unresolved questions. *Proceedings of the Combustion Institute*, 20:857–870, 1984.